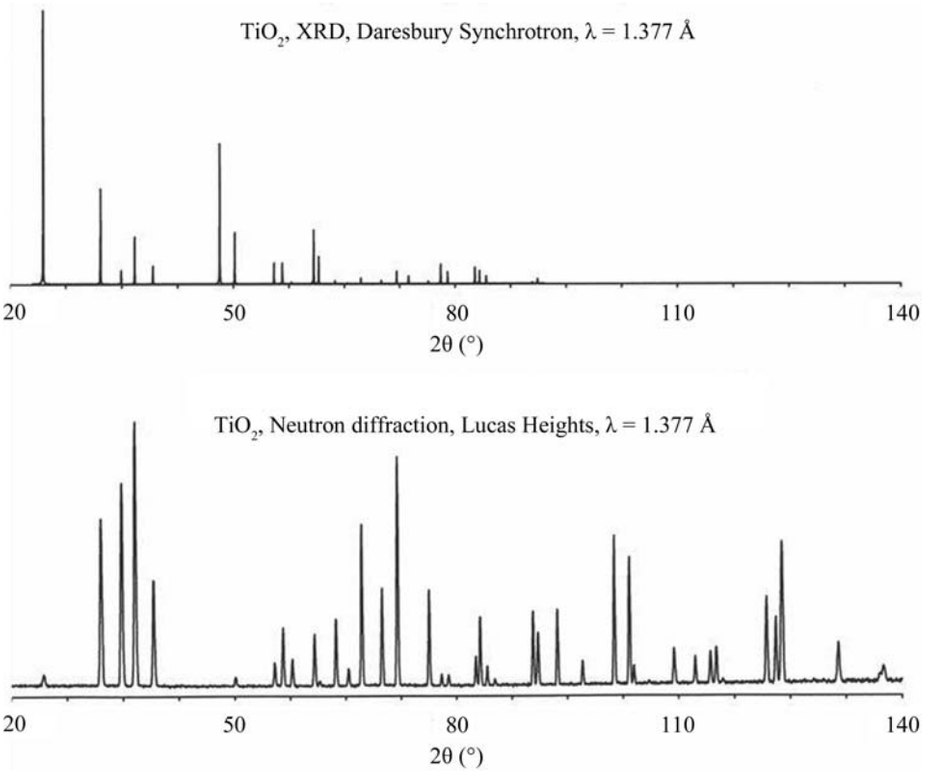

Figure 2.3.2
Comparison of X-ray and neutron powder-diffraction patterns from rutile, TiO_2. The patterns were recorded at the same wavelength, 1.377 Å. The differences between form factors and scattering lengths give rise to large differences in the relative intensities of the different peaks; note also that the fall off in the form factor evident in the X-ray case does not occur for neutrons.

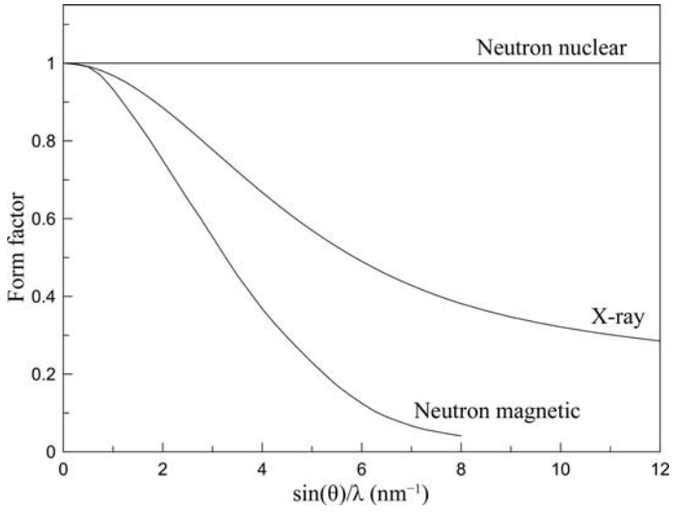

Figure 2.3.3
The magnetic form factor for Mn^{2+} compared with the normalized X-ray form factor and the normalized neutron nuclear scattering length.

of nuclear moments in metallic copper (^{65}Cu) at temperatures below 60 nK (Hakonen *et al.*, 1991).[3]

(*c*) *Low attenuation*: The combination of the small scattering cross sections and generally low cross sections for absorption (notable exceptions are B, Cd and Gd) gives thermal neutrons the ability to penetrate quite deeply into most materials. Indeed, the linear attenuation coefficient for thermal (25 meV) neutrons in Fe is 110 m^{-1}, and for neutrons in Al it is only about 9.8 m^{-1}; the implication is that it takes about 10 cm of Al to reduce the intensity by a factor 1/*e*. The fact that neutrons are so little attenuated by these materials makes it easier to design large and complex sample-environment chambers which may be used for *in situ* studies at high temperature, under pressure or stress, in magnetic fields, and in reaction cells (Chapters 2.6–2.9; Chapter 3 in Kisi & Howard, 2008). Neutron powder diffraction is well suited to quantitative phase analysis (QPA, see Chapter 3.9 and Chapter 8 in Kisi & Howard, 2008); as pointed out in Chapter 8, Section 8 of Kisi & Howard (2008), neutron QPA provides a better sampling ability and is less prone to microabsorption errors than the X-ray technique; indeed, neutron diffraction was the method employed in one of the earliest and most convincing demonstrations of the Rietveld method in QPA (Hill & Howard, 1987). Another advantage conferred by the deep penetration of neutrons is the ability to probe below the surface of samples to measure such aspects as structure, phase composition and stress; a particular example is the application to the analysis of zirconia ceramics (Kisi *et al.*, 1989) where the surface composition (as would be measured by X-rays) is unrepresentative of the bulk. A downside of the small scattering cross sections (along with neutron sources of limited 'brightness') is that relatively large samples may be required.

(*d*) *Low energy*: We note from equation (2.3.1) that, for a specified wavelength, the energy of the neutron is much less than that for lighter probes, such as electrons or photons. This is critically important for studying inelastic processes (*e.g.* measurement of phonon dispersion curves), but is usually not a factor in neutron powder diffraction.[4]

Neutron sources, in common with synchrotrons, are large national or international facilities, set up to cater for scientists from external laboratories. There are usually well defined access procedures, involving the submission and peer review of research proposals. Visiting users are usually assisted in their experiments by in-house staff. In some cases external users can mail in their samples for collection of diffraction data by the resident staff.

2.3.2. Neutrons and neutron diffraction – pertinent details

2.3.2.1. *Properties of the neutron*

The basic properties of the neutron are summarized in Table 2.3.1.

[3] This study depends on the spin-dependent scattering lengths rather than magnetic scattering *per se*.

[4] However, if the incident beam is monochromatic, a crystal monochromator placed in the diffracted beam can be used to exclude inelastic scattering from the 'background'.

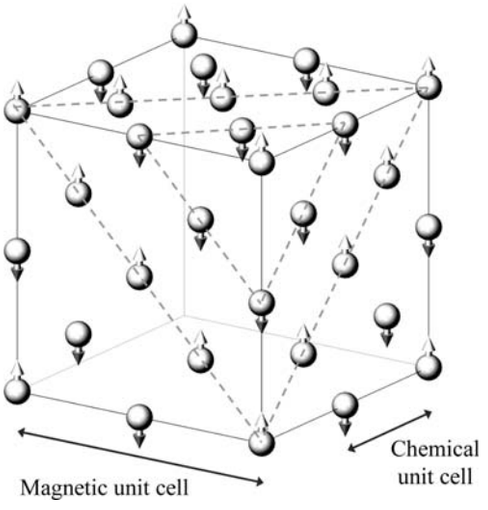

Figure 2.3.4
Magnetic structure for MnO proposed by Shull *et al.* (1951). The figure shows only the Mn atoms, and indeed only those Mn atoms located on the visible faces of the cubic cell. [From Shull *et al.* (1951), redrawn using *ATOMS* (Dowty, 1999).]

Table 2.3.1
Properties of the neutron (adapted from Kisi & Howard, 2008)

Mass (m)	1.675×10^{-27} kg
Charge	0
Spin	$\frac{1}{2}$
Magnetic moment (μ_n)	$-1.913\ \mu_N$
Wavelength (λ)	h/mv
Wavevector (**k**)	Magnitude $2\pi/\lambda$
Momentum (**p**)	$\hbar\mathbf{k}$
Energy (E)	$(1/2)mv^2 = h^2/2m\lambda^2$

2.3.2.2. *Neutron scattering lengths*

The scattering lengths of most interest in neutron powder diffraction are those for coherent elastic scattering, $b_{\rm coh}$, often abbreviated to b. As already mentioned, there is no angle (Q) dependence, since the scattering from the nucleus is isotropic. A selection of scattering lengths for different isotopes and different elements is given in Table 2.3.2.

The first thing to note is the variation in scattering length from element to element and indeed from isotope to isotope. The scattering lengths are in most cases positive real numbers, in which case there is a phase reversal of the neutron on scattering, but for some isotopes the scattering lengths are negative, so there is no change in phase on scattering. The scattering lengths are determined by the details of the neutron–nucleus interaction (Squires, 1978).[5] In the event that the neutron–nucleus system is close to a resonance, such as it is for ^{10}B, ^{155}Gd and ^{157}Gd, scattering lengths will be complex quantities and the scattered neutron will have some different phase relationship with the incident one. The imaginary components imply absorption, which is reflected in the very high absorption cross sections, σ_a, for these isotopes.

The total scattering cross section, σ_s, is given by $\sigma_s = 4\pi b_{\rm coh}^2$ when only coherent scattering from a single isotope is involved, which is very nearly the case for oxygen since 99.76% of naturally occurring oxygen is zero-spin ^{16}O. In most cases there is a more substantial contribution from incoherent scattering, which may be either spin or isotope incoherent scattering. Spin incoherent scattering arises because the scattering length depends on the relative orientation of the neutron and nuclear spins, parallel and antiparallel arrangements giving rise to scattering lengths b_+ and b_-, respectively. Isotope incoherent scattering arises because of the different scattering of neutrons from different isotopes of the same element. In almost all circumstances (except, for example, at the extraordinarily low temperatures mentioned in Section 2.3.1) the distributions of spins and isotopes are truly random, which means that there is no angle dependence in this scattering: this is sometimes described as Laue monotonic scattering.

[5] It is evident from Fig. 2.3 in this reference that even for an attractive interaction between neutron and nucleus positive scattering lengths will predominate.

When b varies from nucleus to nucleus (even considering just a single element), the coherent scattering is determined by the average value of b, that is $b_{\rm coh} = \overline{b}$, $\sigma_{\rm coh} = 4\pi(\overline{b})^2$, and the average incoherent cross section is given by $\sigma_{\rm inc} = 4\pi[\overline{b^2} - (\overline{b})^2]$. The total scattering cross section σ_s is the sum of the two cross sections (Squires, 1978; see also Section 2.3.2 in Kisi & Howard, 2008). For the particular case of a nucleus with spin I, the states $I + 1/2$ and $I - 1/2$ give scattering determined by b_+ and b_-, respectively, and have multiplicities $2I + 2$ and $2I$, respectively, from which it follows that

$$b_{\rm coh} = \overline{b} = \frac{I+1}{2I+1}b_+ + \frac{I}{2I+1}b_-,$$
$$b_{\rm inc}^2 = \left[\overline{b^2} - (\overline{b})^2\right] = \frac{I(I+1)}{(2I+1)^2}(b_+ - b_-)^2.$$

More information, including a comprehensive listing of scattering lengths, can be found in Section 4.4.4 of *International Tables for Crystallography* Volume C (Sears, 2006). This listing presents the spin-dependent scattering lengths *via* $b_{\rm coh}$ and $b_{\rm inc}$ as just defined. Other compilations can be found in the *Neutron Data Booklet* (Rauch & Waschkowski, 2003), and online through the Atominstitut der Österreichischen Universitäten, Vienna, at http://www.ati.ac.at/~neutropt/scattering/table.html. In addition, the majority of computer programs used for the analysis of data from neutron diffraction incorporate, for convenience, a list of $b_{\rm coh}$ values for the elements.

2.3.2.3. *Refractive index for neutrons*

The coherent scattering lengths of the nuclei determine the refractive index for neutrons through the relationship (Squires, 1978)

$$n = 1 - \frac{1}{2\pi}\lambda^2 N b_{\rm coh}, \tag{2.3.4}$$

where N is the number of nuclei per unit volume. For elements with positive values of the coherent scattering length the refractive index is slightly less than one, and that leads to the possibility of total external reflection of the neutrons by the element in question. In fact, when the coherent scattering length is positive, neutrons will undergo total external reflection for glancing angles less than a critical angle γ_c given by

$$\cos\gamma_c = n = 1 - \frac{1}{2\pi}\lambda^2 N b_{\rm coh}, \tag{2.3.5}$$

which, since γ_c is small, reduces to

$$\gamma_c = \lambda\left(\frac{N b_{\rm coh}}{\pi}\right)^{1/2}. \tag{2.3.6}$$

It can be seen that the pertinent material quantity is $Nb_{\rm coh}$, the 'coherent scattering length density'; for materials comprising more than one element this is the quantity that would be

Table 2.3.2
Coherent scattering lengths and absorption cross sections (for 25 meV neutrons) for selected isotopes

Data are taken from Section 4.4.4 of Volume C (Sears, 2006). Where not stated, the values are for the natural isotopic mix. The X-ray atomic form factors, f, evaluated at $Q = 1.2\pi$ Å^{-1}, are included for comparison.

Element	Isotope	b_{coh} (fm)	$\sigma_{s(tot)}$ (10^{-24}cm^2)	σ_a (10^{-24}cm^2)	f	Isotopic abundance (%)
H		−3.7390 (11)	82.02 (6)	0.3326 (7)	0.25	
	1	−3.7406 (11)	82.03 (6)	0.3326 (7)		99.985
	2	6.671 (4)	7.64 (3)	0.000519 (7)		0.015
	3	4.792 (27)	3.03 (5)	0		—
B		5.30 (4) − 0.213 (2)*i*	5.24 (11)	767 (8)	1.99	
	10	−0.1 (3) − 1.066 (3)*i*	3.1 (4)	3835 (9)		20.0
	11	6.65 (4)	5.78 (9)	0.0055 (33)		80.0
C		6.6460 (12)	5.551 (3)	0.00350 (7)	2.50	
	12	6.6511 (16)	5.559 (3)	0.00353 (7)		98.90
	13	6.19 (9)	4.84 (14)	0.00137 (4)		1.10
O		5.803 (4)	4.232 (6)	0.00019 (2)	4.09	
Ti		−3.370 (13)	4.06 (3)	6.43 (6)	13.2	
	46	4.725 (5)	2.80 (6)	0.59 (18)		8.2
	47	3.53 (7)	3.1 (2)	1.7 (2)		7.4
	48	−5.86 (2)	4.32 (3)	8.30 (9)		73.8
	49	0.98 (5)	3.4 (3)	2.2 (3)		5.4
	50	5.88 (10)	4.34 (15)	0.179 (3)		5.2
V		−0.3824 (12)	5.10 (6)	5.08 (2)	14.0	
Ni		10.3 (1)	18.5 (3)	4.49 (16)	18.7	
	58	14.4 (1)	26.1 (4)	4.6 (3)		68.27
	60	2.8 (1)	0.99 (7)	2.9 (2)		26.10
	61	7.60 (6)	9.2 (3)	2.5 (8)		1.13
	62	−8.7 (2)	9.5 (4)	14.5 (3)		3.59
	64	−0.37 (7)	0.017 (7)	1.52 (3)		0.91
Cu		7.718 (4)	8.03 (3)	3.78 (2)	19.9	
	63	6.43 (15)	5.2 (2)	4.50 (2)		69.17
	65	10.61 (19)	14.5 (5)	2.17 (3)		30.83
Zn		5.680 (5)	4.131 (10)	1.11 (2)	20.8	
Zr		7.16 (3)	6.46 (14)	0.185 (3)	27.0	
Gd		6.5 (5)	180 (2)	49700 (125)	45.9	
	155	6.0 (1) − 17.0 (1)*i*	66 (6)	61100 (400)		14.8
	157	−1.14 (2) − 71.9 (2)*i*	1044 (8)	259000 (700)		15.7
Pb		9.405 (3)	11.118 (7)	0.171 (2)	60.9	

computed. Since the critical angle for total external reflection is proportional to the neutron wavelength, it is convenient to express this as degrees per ångstrom of neutron wavelength. These are important considerations in the design and development of neutron guides (Section 2.3.3.4).

2.3.2.4. *Neutron attenuation*

Neutron beams are attenuated by coherent scattering, incoherent scattering and true absorption. The cross sections for all these processes are included in the tables cited above. For powder diffraction, the coherent scattering is usually small because it takes place only in that small fraction of crystallites correctly oriented for Bragg reflection; the other processes, however, take place throughout the sample.

If a particular scattering entity i with scattering cross sections $(\sigma_i)_{inc}$ and $(\sigma_i)_{abs}$ is present at a number density N_i, then the contribution it makes to the linear attenuation coefficient μ is $\mu_i = N_i[(\sigma_i)_{inc} + (\sigma_i)_{abs}]$. If the mass is M_i, then the density is simply $\rho_i = N_i M_i$, so we have the means to evaluate the mass absorption coefficient $(\mu/\rho)_i$. The calculation of absorption for elements, compounds and mixtures commonly proceeds by the manipulation of mass absorption coefficients, in the same manner as is employed for X-rays (see Section 2.4.2 in Kisi & Howard, 2008).

2.3.2.5. *Magnetic form factors and magnetic scattering lengths*

For a complete treatment of the magnetic interaction between the neutron and an atom carrying a magnetic moment, and the resulting scattering, the reader is referred elsewhere [Marshall & Lovesey, 1971; Squires, 1978; Section 6.1.2 of Volume C (Brown, 2006*a*)]. The magnetic moment of an atom is associated with unpaired electrons, but may comprise both spin and orbital contributions. The magnetic interaction between the neutron and the atom depends on the directions of the scattering vector and the magnetic moment vector according to a triple vector product. The direction of polarization of the neutron must also be taken

into account. For an unpolarized incident beam, the usual case in neutron powder diffraction, it is a useful consequence of the triple vector product that the magnetic scattering depends on the sine of the angle that the scattering vector makes with the magnetic moment on the scattering atom (see Section 2.3.4 and Chapter 7 in Kisi & Howard, 2008). The extent of the unpaired electron distribution (usually outer electrons) implies that the scattering diminishes as a function of Q, an effect that can be described by a magnetic form factor. For a well defined direction for the magnetic moment $\mathbf{M}$, and with a distribution of moment that can be described by a normalized scalar $m(\mathbf{r})$, the form factor as a function of the scattering vector $\mathbf{h}$ [defined in equation (1.1.17) in Chapter 1.1][6] is the Fourier transform of $m(\mathbf{r})$,

$$f(\mathbf{h}) = \int m(\mathbf{r}) \exp(2\pi i \mathbf{h} \cdot \mathbf{r})\, \mathrm{d}\mathbf{r},$$

where $m(\mathbf{r})$ can comprise both spin and orbital contributions [Section 6.1.2 of Volume C (Brown, 2006*a*)]. The tabulated form factors are based on the assumption that the electron distributions are spherically symmetric, so that $m(\mathbf{r}) = m(r) = U^2(r)$, where $U(r)$ is the radial part of the wave function for the unpaired electron. In the expansion of the plane-wave function $\exp(2\pi i \mathbf{h} \cdot \mathbf{r})$ in terms of spherical Bessel functions, we find that the leading term is just the zeroth-order spherical Bessel function $j_0(2\pi hr)$ with a Fourier transform

$$\langle j_0(h) \rangle = 4\pi \int_0^\infty U^2(r) j_0(2\pi hr) r^2\, \mathrm{d}r.$$

This quantity is inherently normalized to unity at $h = 0$, and may suffice to describe the form factor for spherical spin-only cases. In other cases it may be necessary to include additional terms in the expansion, and these have Fourier transforms of the form

$$\langle j_l(h) \rangle = 4\pi \int_0^\infty U^2(r) j_l(2\pi hr) r^2\, \mathrm{d}r$$

with l even; these terms are zero at $h = 0$ (Brown, 2006*a*). In practice these quantities are evaluated using theoretical calculations of the radial distribution functions for the unpaired electrons [Section 4.4.5 of Volume C (Brown, 2006*b*)].

Form factors can be obtained from data tabulated in Section 4.4.5 of Volume C (Brown, 2006*b*). Data are available for elements and ions in the 3*d*- and 4*d*-block transition series, for rare-earth ions and for actinide ions. These data are provided by way of the coefficients of analytical approximations to $\langle j_l(h) \rangle$, the analytical approximations being

$$\langle j_0(s) \rangle = A \exp\left(-as^2\right) + B \exp\left(-bs^2\right) + C \exp\left(-cs^2\right) + D$$

and for $l \neq 0$

$$\langle j_l(s) \rangle = s^2 \left[A \exp\left(-as^2\right) + B \exp\left(-bs^2\right) + C \exp\left(-cs^2\right) + D\right],$$

where $s = h/2$ in Å^{-1}. These approximations, with the appropriate coefficients, are expected to be coded in to any computer program purporting to analyse magnetic structures. Although the tabulated form factors are based on theoretical wave functions, it is worth noting that the incoherent scattering from an ideally disordered (*i.e.*, paramagnetic) magnetic system will display the magnetic form factor directly.

It is often convenient to define a (Q-dependent) magnetic scattering length

$$p = \left(\frac{e^2\gamma}{2m_e c^2}\right) gJf,$$

where m_e and e are the mass and charge of the electron, γ ($= \mu_n$) is the magnetic moment of the neutron, c is the speed of light, J is the total angular momentum quantum number, and g is the Landé splitting factor given in terms of the spin S, orbital angular momentum L, and total angular momentum quantum numbers by

$$g = 1 + \frac{J(J+1) + S(S+1) - L(L+1)}{2J(J+1)}.$$

For the spin-only case, $L = 0$, $J = S$, so $g = 2$. The differential magnetic scattering cross section per atom is then given by q^2p^2 where $|q| = \sin\alpha$, α being the angle between the scattering vector and the direction of the magnetic moment. This geometrical factor is very important, since it can help in the determination of the orientation of the moment of interest; there is no signal, for example, when the moment is parallel to the scattering vector. Further discussion appears in Chapters 2 (Section 2.3.4) and 7 in Kisi & Howard (2008).

2.3.2.6. *Structure factors*

The locations of the Bragg peaks for neutrons are calculated as they are for X-rays[7] (Section 1.1.2), and the intensities of these peaks are determined by a structure factor, which in the nuclear case is [*cf.* Chapter 1.1, equation (1.1.56)]

$$F_{hkl}^{\text{nuc}} = \sum_{i=1}^{m} b_i T_i \exp(2\pi i \mathbf{h} \cdot \mathbf{u}_i), \tag{2.3.7}$$

where b_i here denotes the coherent scattering length, T_i has been introduced to represent the effect of atomic displacements (thermal or otherwise, see Section 2.4.1 in Kisi & Howard, 2008), $\mathbf{h}$ is the scattering vector for the hkl reflection, and the vectors $\mathbf{u}_i$ represent the positions of the m atoms in the unit cell.

For coherent magnetic scattering, the structure factor reads

$$F_{hkl}^{\text{mag}} = \sum_{i=1}^{m} p_i \mathbf{q}_i T_i \exp(2\pi i \mathbf{h} \cdot \mathbf{u}_i), \tag{2.3.8}$$

where p_i is the magnetic scattering length. The vector $\mathbf{q}_i$ is the 'magnetic interaction vector' and is defined by a triple vector product (Section 2.3.4 in Kisi & Howard, 2008), and has modulus $\sin\alpha$ as already mentioned. In this case the sum needs to be taken over the magnetic atoms only.

As expected by analogy with the X-ray case, the intensity of purely nuclear scattering is proportional to the square of the modulus of the structure factor $|F_{hkl}^{\text{nuc}}|^2$. In the simplest case of a collinear magnetic structure and an unpolarized incident neutron beam, the intensity contributed by the magnetic scattering is proportional to $|F_{hkl}^{\text{mag}}|^2$, and the nuclear and magnetic contributions are additive.

2.3.3. Neutron sources

2.3.3.1. *The earliest neutron sources*

The earliest neutron source appears to have been beryllium irradiated with α-particles (helium nuclei), as emitted for example by polonium or radon. First described as 'beryllium radiation', the radiation from a Po/Be source was identified by

[6] To reiterate, $\mathbf{h} = \mathbf{s} - \mathbf{s}_0$, where $\mathbf{s}_0$ and $\mathbf{s}$ are vectors, each of magnitude $1/\lambda$, defining the incident and scattered beams. Note that $\mathbf{Q} = 2\pi\mathbf{h}$.

[7] The nuclear unit cell is expected to coincide with the X-ray unit cell, but the magnetic unit cell may be larger. So, although the methods of calculation are the same, the larger magnetic cell may give rise to additional (magnetic) Bragg peaks.